Limnol. Oceanogr., 55(1), 2010, 225 238

Double-diffusive convection in Lake Kivu

Martin Schmid,[a,*] Myles Busbridge,[a,1] and Alfred Wüest[a,b]

[a] Eawag, Swiss Federal Institute of Aquatic Science and Technology, Surface Waters Research and Management, Kastanienbaum, Switzerland

[b] Institute of Biogeochemistry and Pollutant Dynamics, ETH Zurich, Zurich, Switzerland

Abstract

Double diffusive staircases with a total of 230 350 mixed layers and sharp interfaces were observed in nine microstructure temperature profiles measured during February 2004 in Lake Kivu. The presence of these staircases at depths > 120 m indicates that diapycnal turbulent mixing is weak and vertical diffusive transport is dominated by double diffusion. Contrary to previously investigated natural or laboratory double diffusive systems, the dissolved gases CO_2 and CH_4 contribute significantly to the density stratification, thereby influencing the formation and the structure of the staircases. The density ratio (i.e., the ratio of the stabilizing effect of dissolved substances to the destabilizing effect of temperature) ranges between 2.0 and 4.5 in large sections of the deep waters, implying a high susceptibility to the formation of staircases. The mixed layers (average thickness 0.48 m) are shown to be in a state of active convection. The average thickness of the interfaces (0.18 m) is surprisingly constant and independent of the large scale stratification. The vertical heat fluxes correlate well with the temperature steps across the interfaces. Lake Kivu receives inflows from subaquatic springs at several depths that maintain the large scale structure of the density stratification and disturb the staircases. In comparison to earlier observations from 1972, the double diffusive heat fluxes appear to have been reduced, leading to a heat accumulation in the deep waters. Conversely, the strengthening of the main chemocline indicates an increased discharge of the subaquatic springs that could be responsible for recent changes in the nutrient cycling and methane production in the lake.

Lake Kivu is one of the large East African Rift lakes, located at 2°N and 29°E on the border between the Democratic Republic of the Congo and Rwanda. It has been estimated that 60 km³ of CH_4 and 300 km³ of CO_2 (gas volumes at standard temperature of 0°C and standard pressure of 1.013×10^5 Pa) are dissolved in the permanently stratified deep water of the lake (Schmid et al. 2005). The accumulation of such high amounts of dissolved gases was possible only because the deep water is effectively decoupled from the lake surface by a steep density gradient at 260-m depth. The diffusive transport through this gradient is very weak and, combined with the slow flushing of the deep water by subaquatic springs, leads to residence times on the order of 800 1000 yr of the water and the gases below the main density gradient (Schmid et al. 2005).

Following the catastrophic gas eruptions from the two Cameroonian crater lakes Nyos (Sigvaldason 1989) and Monoun (Sigurdsson et al. 1987), it was feared that a similar disaster could occur in Lake Kivu. The 5097-km² large catchment area of Lake Kivu is densely inhabited with an average of more than 400 inhabitants km $^{-2}$ (Muvundja et al. 2009). Therefore, a gas eruption from the lake would have the potential to become one of the largest natural disasters in human history. Furthermore, observations made from sediment cores have indicated the occurrences of previous large-scale gas eruptions (Haberyan and Hecky 1987). However, at the current gas concentrations, an extremely high energy input would be required to trigger such a gas release from the main basin. Therefore, its occurrence can be excluded except for the case of a magma eruption directly into the deep water (Schmid et al. 2004*b*). A notable exception is the Kabuno Bay in the northwestern part of the lake, which is separated from the main basin by a shallow sill. There, CO_2 concentrations are near saturation, although fortunately only in a thin layer at shallow depths (Tietze 1978; Tassi et al. 2009).

The methane deposit found in Lake Kivu is an important and valuable energy resource for both bordering countries. A small experimental methane extraction plant was constructed in 1963, supplying methane to a local brewery. Large-scale commercial gas extraction is expected to advance the local electricity supply in the upcoming decades. The first pilot plant has been extracting methane from the lake since October 2008.

Double diffusion is a phenomenon caused by a large difference of two orders of magnitude between the molecular diffusivities of heat and dissolved substances in water. If one of these components is stabilizing the stratification while the other one is destabilizing to a slightly lesser extent, double-diffusive processes can lead to local instabilities and vertical mixing. In general, two different regimes are distinguished: the finger regime and the diffusive regime. In the finger regime, salty and warm water is overlying fresher and cooler water, leading to the formation of blobs of rising freshwater and sinking salty water (Kunze 2003). The finger regime enhances mixing in several regions of the ocean (Schmitt et al. 2005) and leads to an increased apparent diffusivity of salt as compared to heat, which has been exemplified in the Mediterranean Sea by Onken and Brambilla (2003). Conversely, in the diffusive regime, cooler and fresher water is lying on top

*Corresponding author: martin.schmid@eawag.ch

[1] Present address: GHD, Perth, Australia.

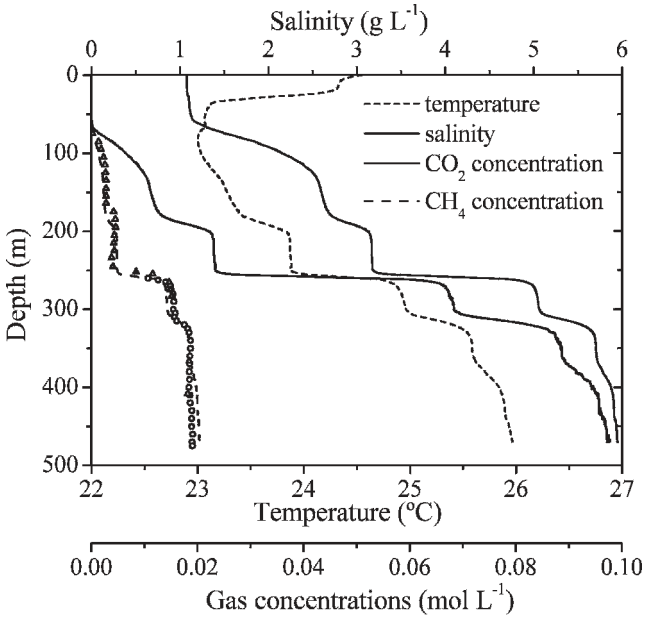

Fig. 1. Vertical profiles of temperature, salinity, and dis solved CO_2 and CH_4 in Lake Kivu observed in February 2004 (Schmid et al. 2005). The CH_4 profile shown here and used in the calculations was set proportional to the CO_2 concentrations in order to avoid unrealistic gradients due to the scatter in the measured values and slightly deviates from the observed data (open circles and triangles).

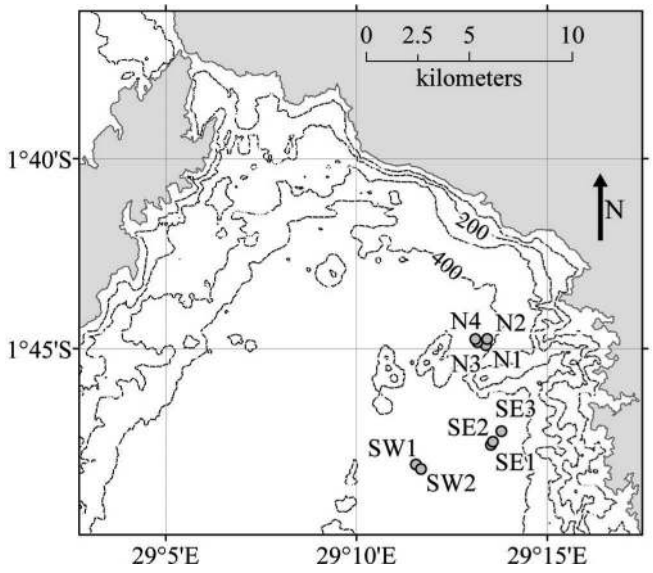

Fig. 2. Locations of the nine microstructure profiles in the northern part of Lake Kivu. The dotted lines depict hypsographs at 100 , 200 , 300 , and 400 m depth.

of warmer and saltier water, with the apparent diffusivity of heat being significantly enhanced compared to that of salts and other dissolved substances (Kelley et al. 2003).

In both regimes, double-diffusive staircases can be formed, which are series of mixed layers separated by interfaces with steep gradients. Double-diffusive staircases have been observed in several lakes, such as Lake Vanda (Hoare 1966) and Lake Nyos (Schmid et al. 2004*a*). Lake Nyos is the first natural system where a double-diffusive staircase was surveyed from its formation to its disappearance (A. Wüest unpubl.). Double-diffusive convection in Lake Kivu was first described by Newman (1976), who observed about 150 mixed layers with thicknesses of 0.5 2.0 m.

In Lake Kivu, the vertical profiles of temperature and dissolved substances are favorable for the diffusive regime (Fig. 1). Temperature is increasing from a minimum of about 23°C at 90-m depth to approximately 26°C at the maximum depth of 485 m, destabilizing the water column. In the same depth range, salinity is increasing from 1.1 g L 1 at the lake surface to 6.0 g L 1 in the deepest reaches. Additionally, in Lake Kivu, double-diffusive processes are influenced by the presence of dissolved gases. Both CO_2 and CH_4 concentrations increase with depth, reaching maximum values of about 100 and 20 mmol L 1, respectively (Fig. 1). CO_2 increases the density of the water, while dissolved CH_4 decreases water density because of its high partial molar volume in water. In summary, there are two stabilizing (salts and CO_2) and two destabilizing (temperature and CH_4) components affecting the stratification in the deep water of the lake. Since the dissolved salts and gases have similar transport properties, they can be grouped together as discussed further below. The situation is therefore different from that in Lake Banyoles, where the effect of suspended particles with different transport properties had to be included as a third component for the density structure (Sánchez and Roget 2007).

The projected large-scale methane extraction is expected to significantly disturb the density stratification of Lake Kivu and therefore the forcing conditions for double-diffusive convection (A. Wüest unpubl.). The objective of this study is to delineate the state of the double-diffusive staircase in this unique natural laboratory before any large-scale anthropogenic interference, based on a detailed analysis of nine temperature microstructure profiles measured in February 2004. Further objectives include evaluating the importance of double diffusion to the heat fluxes in the lake, assessing the changes in the stratification and the double-diffusive staircase since the observations of Newman (1976), identifying the processes that support the formation and destruction of the staircases, and evaluating the influence of the dissolved gases on the double-diffusive processes in Lake Kivu.

Methods

CTD profiles Thirteen vertical profiles of temperature and conductivity (CTD) were measured in February 2004 in the northern half of Lake Kivu with a Sea-Bird SBE-19 that was additionally equipped with a Sea-Bird SBE-22B combined pH and oxygen sensor.

Microstructure profiles Ten temperature microstructure profiles were measured on 18 20 February 2004 with a free-falling adapted Sea-Bird SBE 9 microstructure probe at the locations indicated in Fig. 2. The probe and measurement methods are described in detail by Kocsis et al. (1999). The probe was equipped with a pressure sensor and

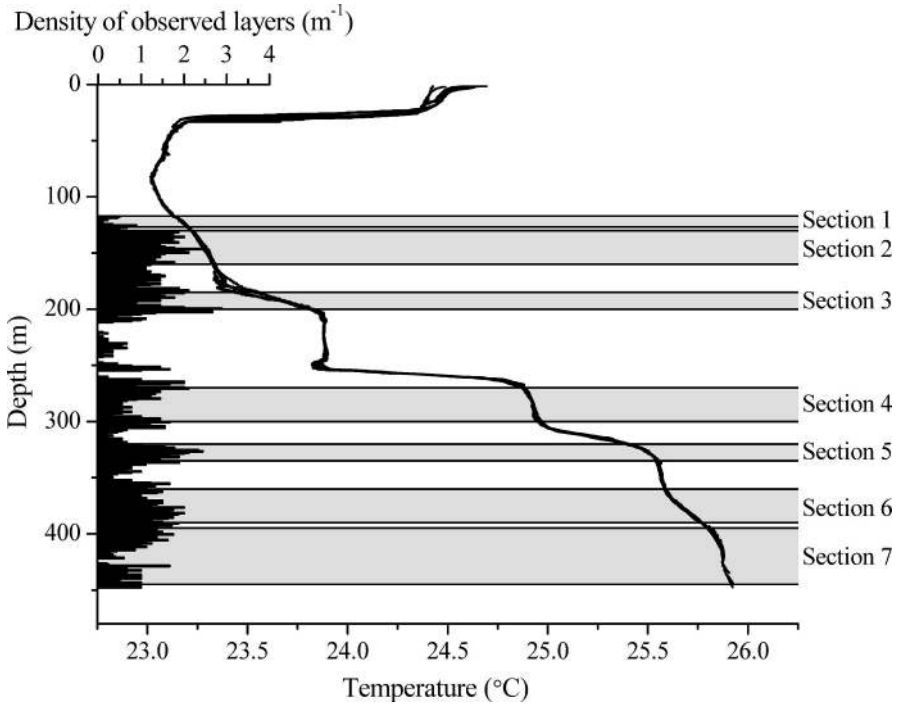

Fig. 3. Nine vertical microstructure temperature profiles observed in February 2004 at the positions shown in Fig. 2. The gray bars mark seven sections for which a more detailed statistical analysis was made. The black histogram shows the average number of observed mixed layers per meter depth in the analyzed profiles.

two Thermometrics FP07 microstructure thermistors with a resolution of ~ 0.02 mK (Kocsis et al. 1999), which was achieved through a built-in pre-emphasis procedure (Mudge and Lueck 1994), enhancing the resolution of temperature differences. The fall rate of the probe, ranging between 0.1 and 0.2 m s ^{1}, combined with a sampling frequency of 96 Hz, resulted in a vertical resolution of 1 2 mm. The nominal response time of the thermistors is 7 ms. The true response time for the given falling speeds was approximately 12 15 ms (Gregg and Meagher 1980). One profile showed significant disturbances that might have been due to strong wave action and was excluded from the analysis presented here. One profile was stopped at a depth of 358 m because of an upcoming storm. The other eight profiles all extended from the surface to depths between 410 and 465 m. A few sections with disturbed signals were cut from the profiles. The absolute temperatures of the two microstructure thermistors were linearly corrected to agree with the temperature of the calibrated slow temperature sensor mounted on the profiler, while depths were corrected by 2.5 m in order to agree with the CTD profiles. The corrected profiles retrieved from the two fast-response thermistors were nearly identical. In the analysis presented here, the data from only one of the thermistors were evaluated, while the other was used as a reference to check whether some unexpected signals were correct.

Data analysis The upper and lower boundaries of observed mixed layers were identified and marked visually using a graphical user interface programmed in Matlab. A mixed layer was identified only if its vertical extent exceeded 0.03 m. Statistical analysis of the profiles was performed using R 2.9.0 and Origin Pro 8.0.

Results

Density stratification and susceptibility to double diffusion Figure 3 shows a compilation of all nine microstructure profiles. The profiles were identical within about 0.01°C, except for the epilimnion and the segments just above the two main thermoclines at 180- and 250-m depth. These two segments are influenced by intrusions of cooler water entering the lake near the northern shore, as discussed in more detail below.

The vertical temperature profiles exhibit a minimum at a depth of 84 m. Temperature increases with depth beyond this minimum, destabilizing the stratification. However, the stratification is stabilized by the vertical gradients of salinity and dissolved CO_2 (Fig. 1). The total stability N^2 of the density stratification is given by (Schmid et al. 2004*b*):

$$N^2 = g\left[-\alpha\left(\frac{\partial T}{\partial z} - \Gamma\right) + \beta_S \frac{\partial S}{\partial z} + \beta_{CO_2} \frac{\partial [H_2CO_3]}{\partial z} + \beta_{CH_4} \frac{\partial [CH_4]}{\partial z}\right] \quad (1)$$

Here, z is the depth (m); T is temperature (°C); S is salinity (g L ^{1}); $[H_2CO_3]$ and $[CH_4]$ are the concentrations of

dissolved carbon dioxide (not including bicarbonate and carbonate, which are part of S) and methane (mol L $^{-1}$), respectively; and g is the gravitational acceleration (m s $^{-2}$). α (K $^{-1}$) and Γ (K m $^{-1}$) are the thermal expansivity and the adiabatic temperature gradient as a function of temperature, pressure, and salinity (Chen and Millero 1986). β_S (0.75×10^{-3} L g $^{-1}$), β_{CO_2} (0.0125 L mol $^{-1}$), and β_{CH_4} (-0.020 L mol $^{-1}$) are the contraction coefficients for the dissolved salts, CO_2 and CH_4 (Schmid et al. 2004*b*). N^2 ranges between 10^{-6} and 10^{-3} s $^{-2}$ throughout the profile below 100-m depth (Fig. 4). This high stability suppresses turbulent diffusion and thus allows the formation of the observed double-diffusive staircases.

The density ratio R_ρ is used as a characteristic dimensionless number for double-diffusive systems. For the case of the diffusive regime, it is usually defined as the ratio of the stabilizing density gradient due to salinity to the destabilizing density gradient due to temperature (Turner 1973):

$$R_\rho = \frac{\beta_S \frac{\partial S}{\partial z}}{\alpha\left(\frac{\partial T}{\partial z} - \Gamma\right)} \tag{2}$$

Double-diffusive staircases have been typically observed for $1 < R_\rho < 10$ (Kelley et al. 2003). In the case of Lake Nyos (Schmid et al. 2004*a*), a term defining the contribution of CO_2 was added to the definition of R_ρ, while in the case of Lake Kivu, a fourth term is required to account for the effect of dissolved CH_4. As CH_4 decreases the density of water, increasing CH_4 concentrations with depth, as observed in Lake Kivu, have a destabilizing effect on density. However, we suggest including the CH_4 term with the other stabilizing components because its diffusivity (Lide 2009) in water (1.84×10^{-9} m^2 s $^{-1}$ at 25°C) is similar to that of CO_2 (1.91×10^{-9} m^2 s $^{-1}$) and salts (ranging from 0.71×10^{-9} m^2 s $^{-1}$ for Mg^{2+} to 1.96×10^{-9} m^2 s $^{-1}$ for K^+ for the major ions in Lake Kivu). We infer that CH_4 reduces the total stabilizing effect of the slowly diffusing components rather than increasing the destabilizing effect of temperature, which diffuses two orders of magnitude faster. This leads to the following definition for R_ρ for Lake Kivu, similar to that derived by Griffiths (1979) for multiple salt components:

$$R_\rho = \frac{\beta_S \frac{\partial S}{\partial z} + \beta_{CO_2} \frac{\partial [H_2CO_3]}{\partial z} + \beta_{CH_4} \frac{\partial [CH_4]}{\partial z}}{\alpha\left(\frac{\partial T}{\partial z} - \Gamma\right)} \tag{3}$$

It has previously been suggested to subtract the CH_4 term from the temperature term rather than adding it to the salt and CO_2 terms in order to group the two destabilizing components together (Lorke et al. 2004). This would result in ~ 20% lower values for R_ρ. However, it seems more natural to group the components on the basis of the similarity of their diffusivities, which have a direct influence on the transport processes, than to do so on the basis of their effect on stratification. Values for R_ρ range between 2.0 and 4.5 for large sections of the deep waters (Fig. 4), meaning that these sections are highly susceptible to the formation of double-diffusive staircases.

Structure of the observed profiles Figures 5 and 6 show the complete microstructure temperature profiles below 110-m depth. For the data analysis, the profiles were grouped and named according to their geographical location (Fig. 2). N1 to N4 indicate the profiles measured near the northeastern corner of the lake, SW1 and SW2 the western, and SE1 to SE3 the eastern of the two groups further south.

Between 115- and 130-m depth, the mixing regime gradually changed from weakly turbulent to double-diffusive. The first occurrence of an isolated mixed layer appeared at 117-m depth in the SW profiles. Almost continuous double-diffusive staircases were found below 130-m depth except for a few zones with strong density gradients and depth ranges that were disturbed by subaquatic sources.

Negative temperature peaks disturbing the double-diffusive layering were observed between 165- and 185-m depth (up to -0.05 K) and between 245- and 255-m depth (up to -0.07 K). The intensity of these peaks progressively decreased from the N profiles to the SE profiles and the SW profiles, where no significant peaks were registered in the upper of these two ranges. These observations are best explained by the presence of subaquatic springs discharging cooler water into the lake somewhere along the northern shore and stratifying at these depths. The zone inbetween these gradients, from 205- to 245-m depth, is relatively homogeneous. In this zone, large completely mixed layers up to 8.5 m thick were observed.

In the gradient zone between 255- and 262-m depth, neither double-diffusive staircases nor any temperature inversions, indicative for turbulent mixing, were observed. Diffusive heat transport through this interface is probably nearly molecular. The gradient zone between 300- and 320-m depth was free of mixed layers in the N profiles. However, the number of mixed layers observed in this zone increased from north to south. No clear evidence for subaquatic inflows could be detected that could explain the formation of this gradient except for weak (~ -0.01 K) negative temperature peaks above the chemocline in the N profiles and weak positive peaks below the chemocline in the SW profiles.

In the section between 345- and 355-m depth, a clear temperature gradient, with only a few small mixed layers, was observed in the N profiles. However, in the SE profiles, a mixed layer of about 7-m thickness was formed, while a cool-water intrusion produced a negative signal of about -0.06 K in the SW profiles. This cool intrusion, arriving from the southwest, was inferred to have triggered the formation of the thick mixed layer in the SE profiles.

Below 390-m depth, the layers were comparatively small in the northern profiles and up to several meters thick in the SE and SW profiles. Furthermore, the SW profiles contained warm-water intrusions that could explain the increase in the layer thickness toward the south. These intrusions could be the signature of the warm, salty, and CO_2-rich source entering the deep water of the lake at an unknown location.

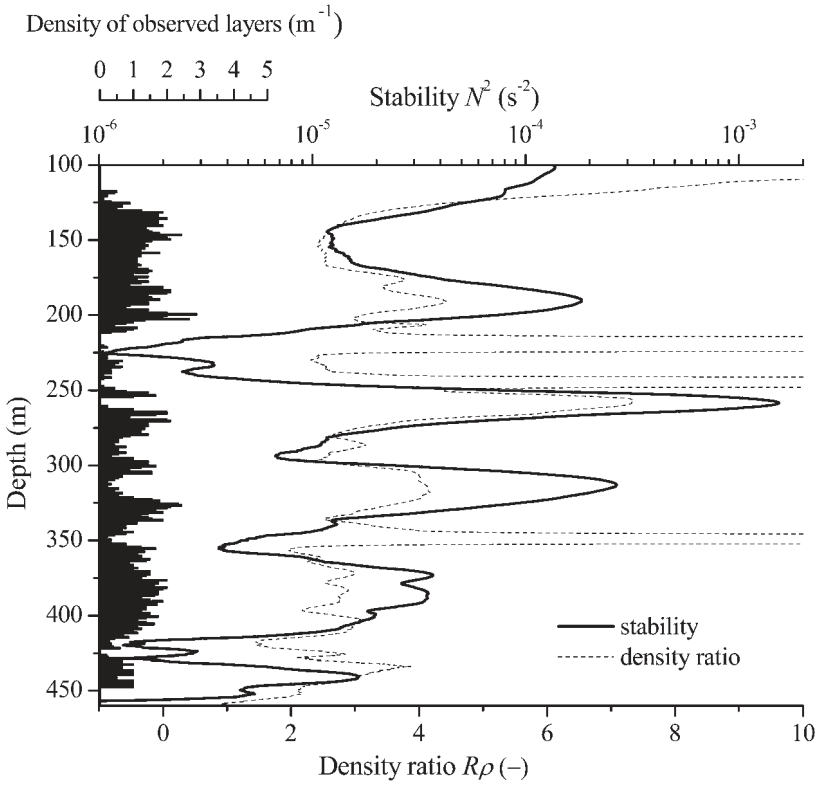

Fig. 4. Vertical profiles of the stability N^2 and the density ratio R_ρ below 100 m depth (average of the four deepest CTD profiles measured in February 2004). The gradients were calculated as running averages of the slopes over 10 m intervals. The black histogram shows the average number of observed layers per meter depth in the analyzed profiles. In a few sections, temperature locally decreases with depth because of intrusions of cooler water. In these sections, R_ρ is not defined, and at their border R_ρ increases to high values as the temperature gradient approaches zero.

Discharge, temperature, and salinity of the subaquatic springs feeding Lake Kivu have previously been estimated with a one-dimensional advective diffusive transport model in order to reproduce the observed vertical profiles of temperature, salinity and dissolved gases (Schmid et al. 2005). The model predicted inflows at six different depths, with the three coolest sources calculated to be at 180-, 250-, and 365-m depth. These depths agree well with the depths at which significant cool intrusions were observed in the microstructure profiles. This supports the hypothesis that the large-scale vertical structure of the temperature profiles is driven mainly by the inflow of subaquatic springs at several depths.

In summary, the microstructure profiles show continuous double-diffusive staircases that are disturbed at some depths by lateral inflows attributed to subaquatic springs. These inflows create strong density gradients that suppress double diffusion and at some depths elicit the formation of exceptionally large mixed layers. The depths and signatures of these intrusions correspond to subaquatic sources previously predicted by means of a modeling approach.

Horizontal coherence of the staircases The horizontal distance between the profiles within each of the three groups (N, SW, and SE) was typically a few hundred meters, whereas the distance between profiles from different groups ranged from 4 to 7 km. Within each group of profiles, horizontally coherent staircases were observed at certain depths, as illustrated in the following examples. In profiles N3 and N4 (200 m apart), coherent layers were observed at 155- to 165-m depth (Fig. 5C), which were similar to profiles N1 and N2 that are 500 to 600 m further east. Strongly correlating layers were observed in profiles SW1 and SW2 (300 m apart) between 285- and 300-m depth (Fig. 6A) and were very similar to the profiles SE1 and SE2 located 4 km to the northeast.

There were no depths where the layer structure was identical in all nine profiles. Therefore, the horizontal extent of individual mixed layers seems to reach, on average, several hundred meters and in some cases up to a few kilometers, resulting in characteristic aspect ratios of ~ 1000. A similar coherence over a few hundred meters was observed in the Beaufort Sea in a staircase with an average mixed layer thickness of ~ 2 m (Padman and Dillon 1987). Two-orders-of-magnitude-higher aspect ratios were found in the Canadian Basin, where double-diffusive layers a few meters in thickness could be tracked over distances of several hundred kilometers (Timmermans et al. 2008).

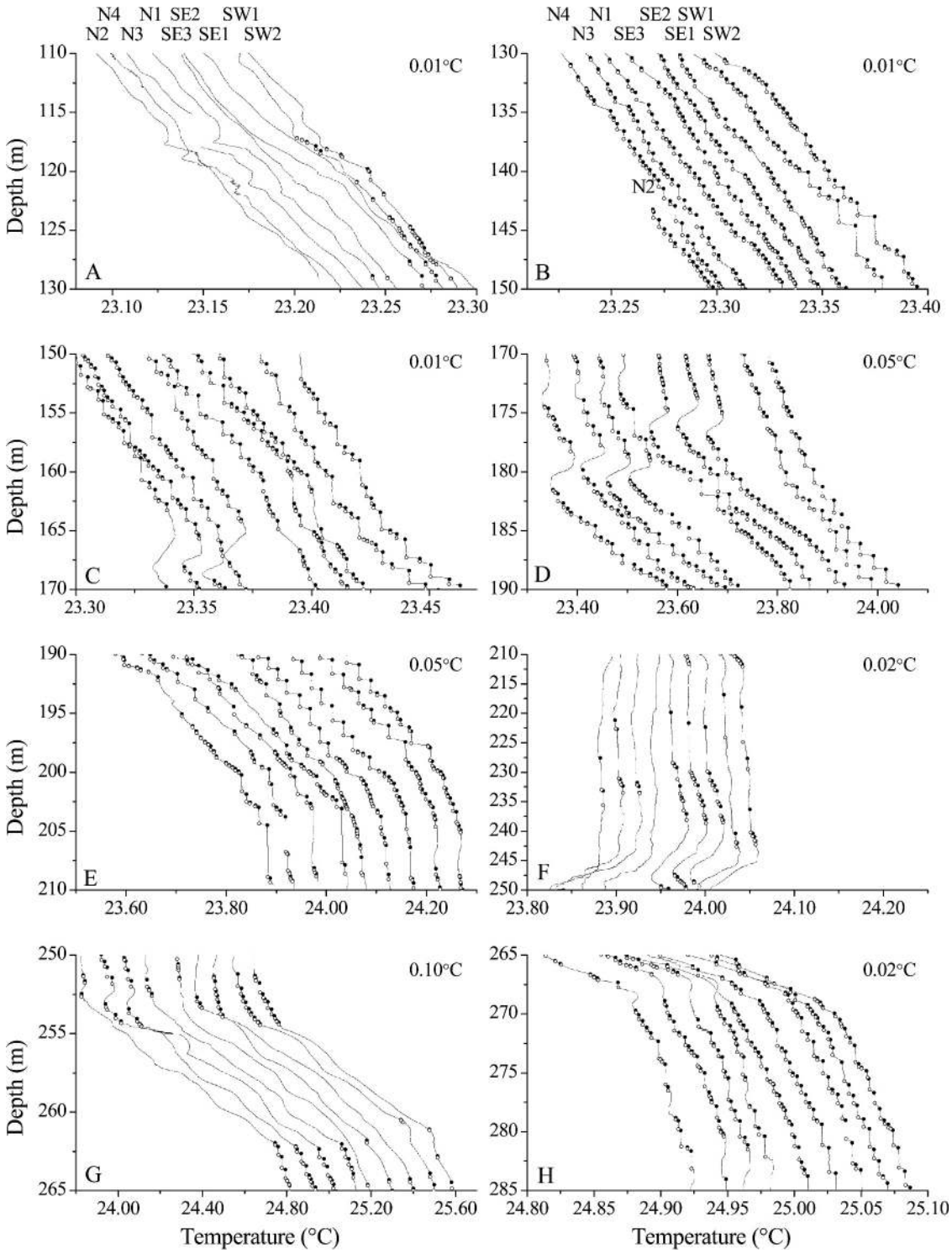

Fig. 5. Microstructure profiles observed in February 2004 between 110 and 285 m depth. The profiles are arranged from north to south. Temperatures of profile N2 are unchanged; each of the following profiles is offset compared to the previous by the value given in the top right of each panel. The upper and lower boundaries of mixed layers are marked with black and white dots, respectively, similar to Fig. 8. Each panel covers a depth range of 20 m, except panels F (40 m) and G (15 m). The temperature scales are adapted to the local temperature gradients in order to achieve an optimal presentation.

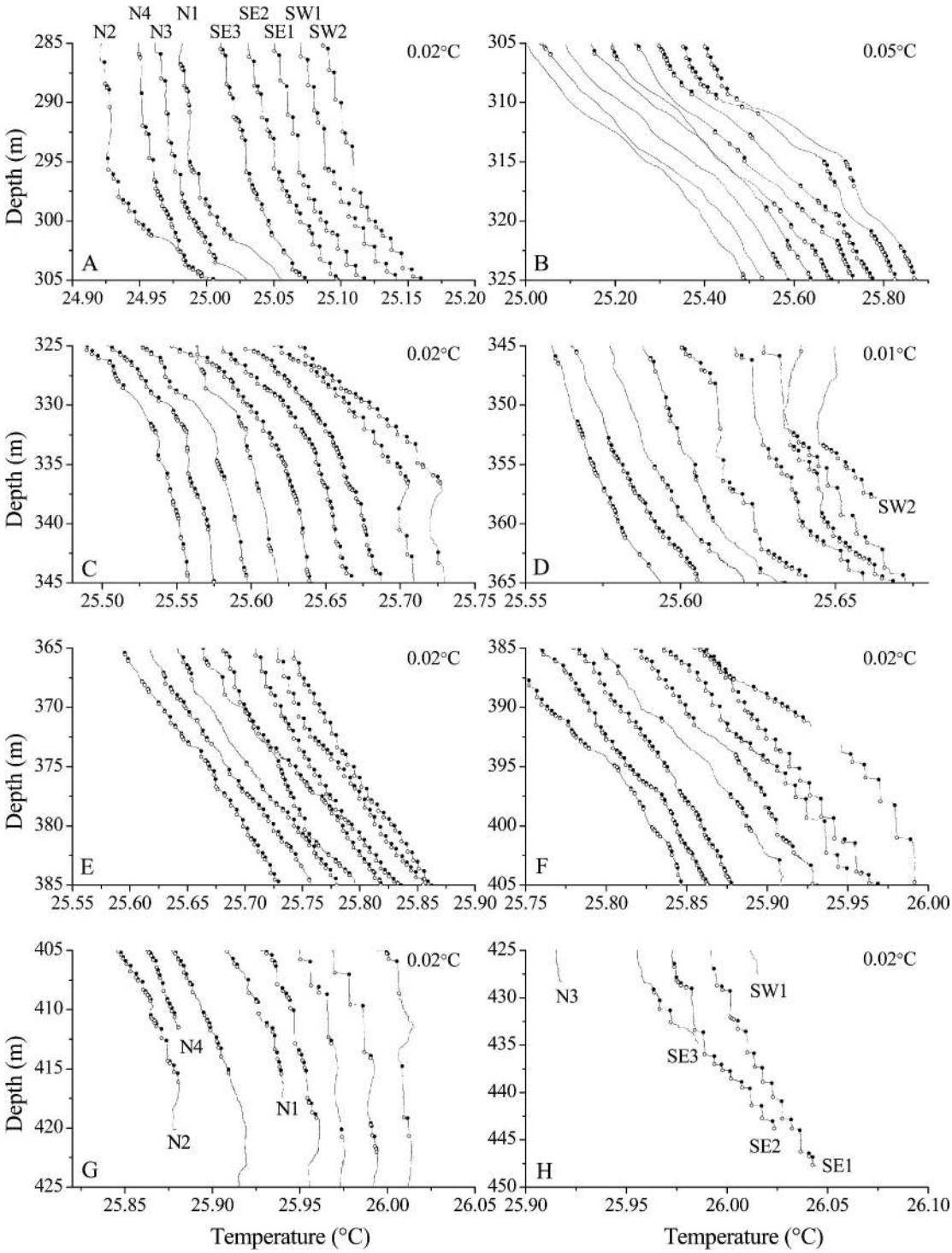

Fig. 6. Same as Fig. 5 for the range between 285 and 450 m depth. Temperatures of profile N2 are unchanged; each of the following profiles is offset compared to the previous by the value given in the top right of each panel. Each panel covers a depth range of 20 m, except for panel H (25 m).

Statistical distribution of stair properties Statistical information about the main properties of the observed stairs is presented in Tables 1 and 2 and Fig. 7. Seven sections with approximately constant vertical gradients of temperature and dissolved substances (Fig. 3) were selected for examining the effect of stratification on the properties of the stairs. The statistics for these seven sections are given in Table 2. Table 3 shows the correlation coefficients between some of the properties of these seven sections.

The average thickness of the mixed layers, H_{mix}, was 0.48 m. The observed distribution could be approximated with a log-normal distribution with a geometric mean of

Table 1. Characteristics of the microstructure profiles.

	Unit	SE1	SE2	SE3	N1	N2	N3	N4	SW1	SW2	Total
Day of Feb 2004		18	18	18	19	19	19	19	20	20	
Maximum depth of profile*	(m)	447.7	443.9	434.8	417.4	420.2	428.3	411.6	427.6	357.8	447.7
Number of mixed layers		345	343	350	233	278	264	339	284	236	2672
Number of interfaces		326	315	321	179	217	231	298	253	210	2350
Number of mixed layers in series†		313	303	304	155	195	211	277	241	199	2198
Average thickness of mixed layers, H_{mix}	(m)	0.58	0.55	0.45	0.43	0.36	0.41	0.38	0.62	0.55	0.48
Maximum layer thickness	(m)	7.57	8.29	8.55	4.55	5.38	2.69	8.35	7.27	5.97	8.55
Average interface thickness, H_{int}	(m)	0.17	0.19	0.21	0.21	0.18	0.19	0.18	0.17	0.16	0.18
Average temperature step across interface, ΔT_{int}	(mK)	4.69	4.55	3.73	4.93	4.73	5.03	4.09	5.62	5.36	4.68
Average SD of temperature within mixed layers, $\sigma_{T,mix}$	(mK)	0.098	0.100	0.091	0.103	0.091	0.115	0.092	0.159	0.145	0.109

* The following sequences >1 m were cut out from the original profiles because of spurious data: SE3: 434.8 435.8 m; N2: 129.1 143.1 m; N3: 115.1 117.9 m; SW1: 391.6 393.2 m, 427.6 465.4 m; SW2: 220.5 222.0 m.
† Number of mixed layers in between two adjacent mixed layers for which heat fluxes according to Kelley (1990) were calculated.

0.29 m and a geometric standard deviation (SD) of 2.68, meaning that about 68% of the values of H_{mix} were within a factor of 2.68 from 0.29 m. The average thickness of the interfaces, H_{int}, between two adjacent mixed layers was 0.18 m (geometric mean: 0.15 m, geometric SD: 1.96). The geometric mean of H_{mix} varied between 0.10 and 0.49 m in the different depth sections, and its logarithm was negatively correlated with R_ρ ($R^2 = 0.74$). In contrast, the geometric mean of H_{int} was surprisingly constant for all sections, varying only between 0.135 and 0.170 m.

The average temperature step across the interfaces, ΔT_{int}, was 4.7 mK (log-normal distribution, geometric mean: 3.1 mK, geometric SD: 2.49). The section-averaged logarithms of ΔT_{int} correlated well with the vertical temperature gradient ($R^2 = 0.84$), which is a direct consequence of the almost constant H_{int}.

The resolution of the temperature profiler of ~ 0.02 mK was sufficient to estimate the standard deviation of temperature within each mixed layer, $\sigma_{T,mix}$, which averaged 0.11 mK. $\sigma_{T,mix}$ can be regarded as a measure for the temperature variability T' of the rising and sinking thermals within a convectively mixed layer.

The average vertical temperature gradient within the mixed layers, dT/dz_{mix}, was 0.23 mK m $^{-1}$. The distribution of dT/dz_{mix} fits best to a Laplace distribution (exponential decay on both sides of the median) with a scale of 0.68 mK m $^{-1}$. Given the typical layer thickness of 0.3 m, this corresponds to variations on the order of 0.2 mK, or two times $\sigma_{T,mix}$. The temperature gradients within the interfaces, dT/dz_{int} (geometric mean: 21.1 mK m $^{-1}$), are approximately two orders or magnitude larger than dT/dz_{mix}.

Discussion

Active convection The observed statistical distributions indicate that the mixed layers are in a state of active convection. The time scale for the molecular diffusion of heat over a distance of 0.14 m (the median of H_{int}) is about 1 d. Consequently, the interfaces must have been actively maintained within the last few days before the measurements. Furthermore, the average of dT/dz_{mix} (0.23 mK m $^{-1}$) slightly exceeds the adiabatic temperature gradient of ~ 0.18 mK m $^{-1}$ (the expected gradient if the layer were completely homogenized), indicating that the mixed layers were nearly homogenized. Finally, according to scaling relations, the temperature fluctuations in a convectively mixed layer should scale with $T' \sim F_{H,mix}^{2/3} H_{mix}^{1/3}$ (Matzner 2001). The observed geometric means of $\sigma_{T,mix}$ for the different depth sections correlated reasonably with geometric means of $F_{H,mix}^{2/3} H_{mix}^{1/3}$ ($R^2 = 0.75$).

Importance of dissolved gases for double diffusion in Lake Kivu Below 100-m depth, the average contribution of the different terms in the numerator of Eq. 3 is 76% for the salinity term, 36% for the CO_2 term, and 12% for the CH_4 term. This means that one-third of the density contribution of CO_2 is neutralized by CH_4, yielding a gas contribution of one-quarter to the stabilizing component in R_ρ. The molecular diffusivities of the dissolved gases are 1.25 to 2 times higher than the molecular diffusivities of the dissolved bicarbonate salts. It has been determined in laboratory studies that such differences can lead to a differential transport of substances through double-diffusive staircases (Griffiths 1979). Therefore, the diffusive transport from the deep water could be slightly faster for the gases than for the salts. However, in Lake Kivu, advective transport via the slow upwelling of water masses dominates over diffusive transport (Pasche et al. 2009). Therefore, we do not expect that the difference in the molecular diffusivities between these substances significantly influences their transport toward the lake surface or the large-scale density stratification.

Heat fluxes The vertical heat fluxes through the thermohaline staircases can be estimated on the basis of the structure of single stairs. Several parameterizations have been suggested in the literature (Fedorov 1988; Fernando 1989; Kelley 1990). Here we use the semiempirical equation proposed by Kelley (1990), which proved successful in predicting heat fluxes through a similar staircase in Lake Nyos (Schmid et al. 2004*a*):

Table 2. Statistics of some special sections of the microstructure profiles.

		Unit	Section 1	Section 2	Section 3	Section 4	Section 5	Section 6	Section 7
Depth range	—	(m)	117–127	130–160	185–200	270–300	320–335	360–390	395–445
Density ratio, R_ρ	Average	(−)	5.57	2.66	4.14	2.85	3.62	2.76	2.58
Stability, N^2	Average	(10^{-6} s^{-2})	68	16	155	14	71	27	9
Large-scale temperature gradient	Average	(mK m^{-1})	6.4	4.0	20.7	3.1	10.7	5.9	2.3
Large-scale salinity gradient	Average	(mg L^{-1} m^{-1})	10.1	2.9	22.5	2.3	9.9	4.1	1.5
Large-scale gradient of CO_2 concentration	Average	(μmol L^{-1} m^{-1})	112	45	483	63	323	153	57
Large-scale gradient of CH_4 concentration	Average	(μmol L^{-1} m^{-1})	24	10	101	13	67	32	12
Number of mixed layers			29	407	198	249	219	339	226
Mixed layer thickness, H_{mix}	Average	(m)	0.137	0.441	0.458	0.783	0.281	0.410	0.636
	Geometric mean	(m)	0.103	0.320	0.305	0.485	0.207	0.313	0.341
	Geometric standard deviation (SD)	(–)	2.06	2.28	2.63	2.96	2.26	2.21	3.03
SD of temperature within mixed layer, $\sigma_{T,mix}$	Average	(mK)	0.048	0.065	0.175	0.105	0.091	0.105	0.108
Temperature gradient within mixed layer, dT/dz_{mix}	Average	(mK m^{-1})	−0.28	0.12	0.22	0.17	0.37	0.52	0.36
	Laplace scale	(mK m^{-1})	0.97	0.40	1.39	0.41	0.86	0.64	0.54
Number of interfaces			18	400	189	230	199	301	186
Thickness of interfaces, H_{int}	Average	(m)	0.221	0.173	0.194	0.177	0.165	0.186	0.181
	Geometric mean	(m)	0.170	0.147	0.136	0.148	0.136	0.152	0.145
	Geometric SD	(–)	2.17	1.74	2.17	1.81	1.81	1.86	1.92
Temperature steps across interfaces, ΔT_{int}	Average	(mK)	2.2	2.2	14.0	2.8	3.9	3.6	2.6
	Geometric mean	(mK)	1.7	1.9	11.4	2.4	3.0	3.1	2.0
	Geometric SD	(–)	2.35	1.77	1.96	1.78	2.12	1.74	2.09
Molecular heat flux through interfaces, $F_{H,mol}$	Average	(mW m^{-2})	6.54	8.90	60.41	11.09	15.79	13.89	11.17
	Geometric mean	(mW m^{-2})	5.75	7.76	50.12	9.55	12.88	12.02	7.94
	Geometric SD	(–)	1.71	1.69	1.95	1.73	1.95	1.71	2.25
Number of mixed layers in series			15	391	184	218	186	284	170
Heat flux through mixed layer, $F_{H,mix}$	Average	(mW m^{-2})	14.1	13.8	138.1	18.4	32.7	26.6	18.6
	Geometric mean	(mW m^{-2})	10.4	12.3	118.6	16.6	24.6	24.1	14.2
	Geometric SD	(–)	2.23	1.69	1.78	1.63	2.10	1.63	2.05
Apparent diffusivity, $K_{T,app}$	Average	(10^{-6} m^2 s^{-1})	0.52	0.85	1.48	1.32	0.79	1.01	1.19
	Geometric mean	(10^{-6} m^2 s^{-1})	0.45	0.73	1.18	1.04	0.69	0.90	0.84
	Geometric SD	(–)	1.73	1.76	2.01	2.05	1.72	1.66	2.24

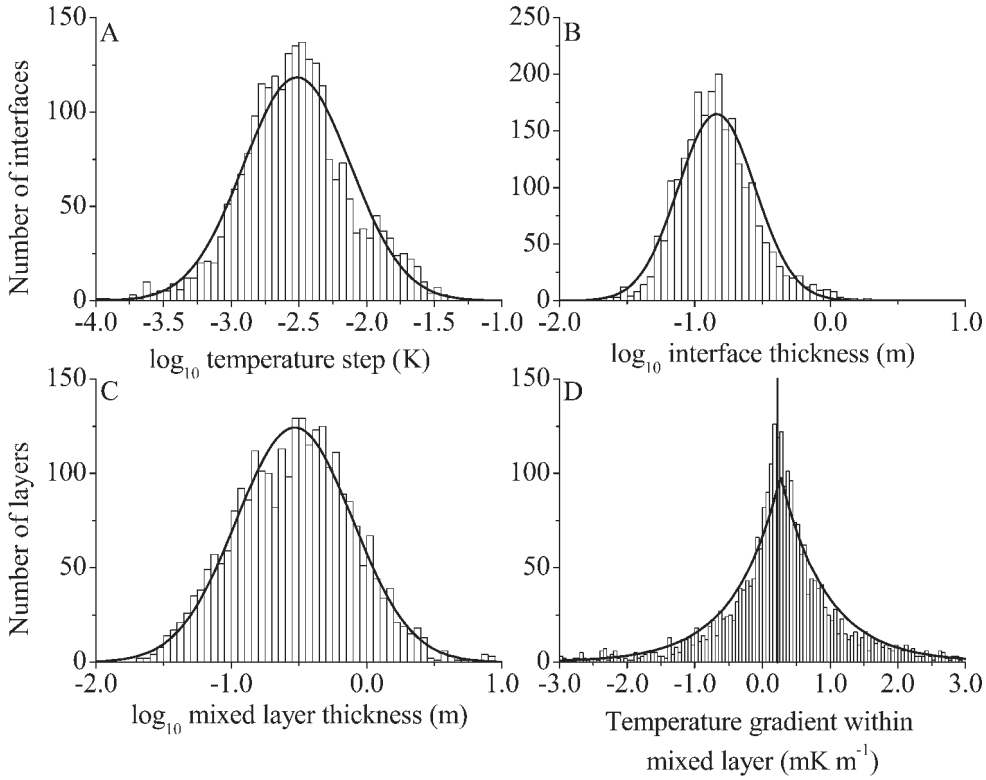

Fig. 7. Histograms and fitted density functions of thicknesses of (A) temperature steps (lognormal distribution, geometric mean: 3.07 mK, geometric SD: 2.49, *n*: 2196), (B) interfaces between two adjacent mixed layers (lognormal distribution, geometric mean: 0.15 m, geometric SD: 1.92, *n*: 2350), (C) mixed layers (lognormal distribution, geometric mean: 0.29 m, geometric SD: 2.68, *n*: 2672), and (D) temperature gradients within the mixed layers (Laplace distribution, median: 0.27 mK m ^{1}, scale: 0.68 mK m ^{1}, *n*: 2672) for all nine evaluated microstructure profiles. The vertical line in (D) marks the adiabatic temperature gradient. Positive gradients denote increasing temperature with depth.

$$F_{H,mix} = \frac{1}{(13 \pm 6)} c_p \rho \left(\frac{g \alpha \Delta T H^3}{D_T \nu} \right)^{0.27 \pm 0.02} \frac{\Delta T D_T}{H} \qquad (4)$$

Here, $F_{H,mix}$ is the upward heat flux through a mixed layer (W m ^{2}); c_p is the heat capacity of water (J K ^{1} kg ^{1}); ρ is water density (kg m ^{3}); ΔT is the temperature step (K) defined as half the difference between the temperature of the layers above and below (Fig. 8); H is the layer thickness (m), including half the interface above and below; D_T is the molecular diffusivity of heat (m^2 s ^{1}); and υ is the kinematic viscosity of water (m^2 s ^{1}). Furthermore, a lower boundary for the heat fluxes was estimated by assuming molecular diffusivity through the interfaces between the convectively mixed layers:

$$F_{H,mol} = c_p \rho D_T \frac{\Delta T_{int}}{H_{int}} \qquad (5)$$

Table 3. Correlation coefficients (R) between the average properties of the seven sections defined in Fig. 3. Asterisks indicate the significance levels (p values) of the correlations.

	dT/dz	dS/dz	log $F_{H,mol}$	log $F_{H,mix}$	log $K_{T,app}$	log $\sigma_{T,mix}$	dT/dz_{mix}	log H_{int}	log ΔT_{int}	log H_{mix}
$R\rho$	0.43	0.62	0.06	0.10	0.57	0.31	0.81*	0.44	0.11	0.86*
dT/dz		0.97***	0.91**	0.92**	0.33	0.62	0.01	0.53	0.92**	0.15
dS/dz			0.81*	0.82*	0.17	0.47	0.23	0.34	0.83*	0.32
log $F_{H,mol}$				0.997***	0.69	0.89**	0.31	0.71	0.997***	0.27
log $F_{H,mix}$					0.67	0.88*	0.30	0.67	0.998***	0.22
log $K_{T,app}$						0.93**	0.66	0.69	0.67	0.87*
log $\sigma_{T,mix}$							0.57	0.74	0.87*	0.64
dT/dz_{mix}								0.71	0.26	0.71
log H_{int}									0.65	0.55
log ΔT_{int}										0.23

*$p < 0.05$; **$p < 0.01$; ***$p < 0.001$.

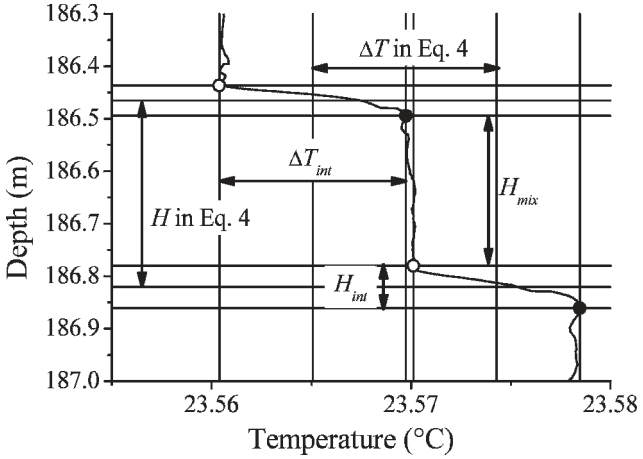

Fig. 8. Example of a mixed layer (from profile SE3) and definitions of the thicknesses of the mixed layers (H_{mix}) and the interfaces (H_{int}) as well as the terms H and ΔT in Eq. 4.

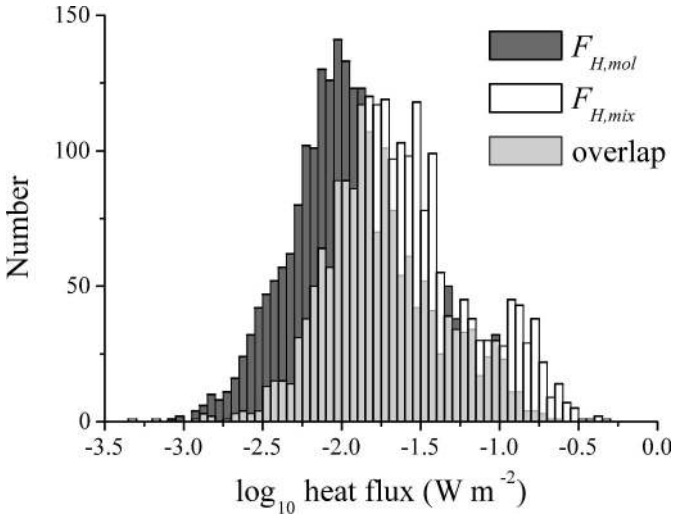

Fig. 9. Histogram of heat fluxes through the double diffusive staircase, calculated either as the molecular heat flux through the interfaces (dark gray bars) or as the convective heat flux through the mixed layer (white bars).

Here, H_{int} (m) and ΔT_{int} (K) are the thickness and the temperature step across each individual interface, respectively. The molecular heat fluxes were calculated for all interfaces between two mixed layers, while the convective heat fluxes were calculated for all mixed layers flanked by two alternate mixed layers (Fig. 9).

The average convective heat flux in the mixed layers was 0.040 W m $^{-2}$ (geometric mean: 0.023 W m $^{-2}$, geometric SD: 2.62), whereas the average molecular heat flux through the interfaces was 0.021 W m $^{-2}$ (log-normal distribution, geometric mean: 0.012 W m $^{-2}$, geometric SD: 2.62). Both values are within the range of heat fluxes (0.016 0.18 W m $^{-2}$) measured in the sediments of the lake (Degens et al. 1973). The average logarithms of the heat fluxes for the seven sections were tightly correlated with each other (R^2 = 0.994) and with the logarithms of ΔT_{int} (R^2 = 0.996 for $F_{H,mix}$ and R^2 = 0.993 for $F_{H,mol}$; Table 3). This could be expected for $F_{H,mol}$ given the approximate constancy of H_{int} but less for $F_{H,mix}$, which is additionally influenced by the more variable H (Eq. 4). The average $F_{H,mix}$ through a series of diffusive stairs in Lake Kivu is $\sim$ 0.01 W m $^{-2}$ for each mK of the average ΔT_{int}. Interestingly, this is also true in the case of Lake Nyos, where heat fluxes were about one order of magnitude larger than in Lake Kivu (Schmid et al. 2004*a*). Assuming that the values estimated by Eq. 4 are correct and that the heat flux through the interfaces is equal to the convective heat flux, the apparent thermal diffusivity through the interfaces would be approximately twice the molecular diffusivity.

Two additional constituents besides $F_{H,mix}$ are required to calculate the heat balance of the lake. First, heat is transported upward via advection caused by the inflow of subaquatic springs in the deep water. The vertical upwelling velocities v_{adv} (m s $^{-1}$) were calculated from the discharges of the subaquatic springs simulated with the model of Schmid et al. (2005). The advective heat fluxes can be estimated as

$$F_{H,adv} = v_{adv} c_p \rho (T(z) - T_{min}) \quad (6)$$

where $T_{min} \sim 23^{\circ}$C is the minimum temperature of the water column. The advective heat fluxes typically range around 0.05 Wm $^{-2}$ in the deep water below 200-m depth. Contrary to the upward fluxes of salts, nutrients, and gases that are dominated by advection (Pasche et al. 2009), the contributions of advection and diffusion are similar for heat because double-diffusive convection allows a much faster diffusive transport of heat than of dissolved substances.

Second, a comparison of vertical temperature profiles from 2002 (Lorke et al. 2004), 2004, and 2007 shows that the temperature of the water column has been continuously warming. The average net heat flux, $F_{H,net}$, required to explain this trend below a depth z_0 was calculated with the heat budget method (Powell and Jassby 1974):

$$F_{H,net}(z_0) = \frac{1}{A_0} c_p \rho \int_{z_{max}}^{z_0} A(z) \frac{\partial T}{\partial t} \, dz \quad (7)$$

Here, A_0 is the cross-sectional area of the lake at the depth z_0. Average values for $F_{H,net}$ are 0.05 0.2 W m $^{-2}$ (Fig. 10), slightly exceeding the sum of the advective and diffusive heat fluxes calculated previously. Furthermore, the observations indicate that the heat input has increased in recent years. In contrast, a comparison with the temperature profiles of Tietze (1980) from 1975 showed only minor changes below the main density gradient (Lorke et al. 2004). The warming trend therefore seems to be a recent phenomenon.

The density difference across the main gradient at 260-m depth corresponds to a temperature difference of $\sim$ 5°C. With a heat input of 0.2 W m $^{-2}$, it would take almost 400 yr to warm up the entire volume below 260 m by 5°C. Therefore, it can be concluded that the observed heat flux is not an imminent threat to the stability of the stratification. The most obvious cause for this warming is a change in the discharge or temperature of the subaquatic springs feeding the lake. However, warming attributed to volcanic activity

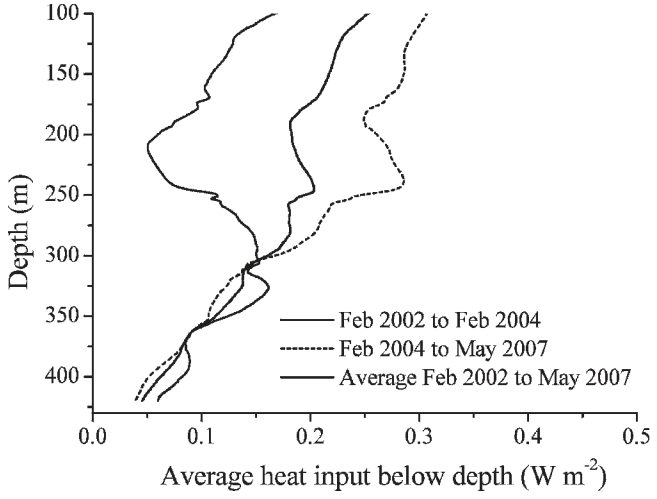

Fig. 10. Average net heat input per cross sectional area at a given depth required to explain the integrated temperature increase below this depth based on CTD temperature profiles measured in February 2002, February 2004, and May 2007.

in the vicinity of the lake should not be a priori excluded. Therefore, it is important to continue monitoring and investigating the causes for this warming. Another possible explanation for the observed trend is a recent decrease of the heat transport by double-diffusive convection, as discussed further below.

The apparent vertical diffusivity of heat, $K_{T,app}$ (m^2 s^{-1}), is defined as the diffusivity that would be required to explain the heat flux based on the large-scale temperature gradient at a specific depth:

$$K_{T,app} = \frac{F_{H,mix}}{c_p \rho \frac{dT}{dz}} \quad (7)$$

The average apparent vertical diffusivity for all mixed layers was 1.1×10^{-6} m^2 s^{-1} (Table 1). Consequently, it is concluded that double diffusion enhances the vertical diffusive heat transport by a factor of 10 relative to molecular diffusivity. This value was remarkably similar in all seven sections, and the geometric standard deviation of $K_{T,app}$ within each section was < 2. Furthermore, $K_{T,app}$ did not correlate with the large-scale temperature gradient. As a consequence, $F_{H,mix}$ increases with the temperature gradient. Thus, the system is to some extent self-regulating, as in the long term double diffusion can be expected to remove excess heat from the deep water.

Comparison with the results of Newman (1976) A comparison of our observations with those made in 1972 by Newman (1976) yielded interesting differences. The most striking is the structure within the main gradient zone. In 1972, the main gradient zone at 260-m depth was approximately 25 m thick and exhibited a double-diffusive staircase. In 2004, this gradient zone was reduced to 7 m and featured no traces of double diffusion or turbulence. This indicates that the forces maintaining this density and temperature gradient have strengthened over time. Observations and model calculations suggest that this gradient layer is maintained by a combination of the slow upwelling of the lake water due to subaquatic springs located in the deep water and the inflow of a strong source of cooler water just above the gradient (Schmid et al. 2005). Therefore, the steepening of this gradient could be attributed to an increased discharge of these springs, which contribute about one-third to the net water input into the lake (Muvundja et al. 2009). They are the main driving force for the recycling of nutrients from the deep water, which is the major source of nutrients for primary production in the surface layer (Pasche et al. 2009). Consequently, an increased discharge of the subaquatic springs would enhance primary productivity and potentially biogenic methane production.

We observed an average H_{mix} of 0.46 and 0.28 m in sections 3 and 5 (Table 2), whereas the same depth ranges had an average layer thickness of > 1 m in 1972. Furthermore, Newman's (1976) estimates for the heat fluxes through the double-diffusive staircases ranged between 0.7 and 1.6 W m^{-2}. However, he used an equation for estimating heat fluxes based on the experiments of Turner (1965), in which the calculated heat fluxes are inversely proportional to the salinity step across the interface. The salinity profiles he used underestimated the salinity gradients by a factor of approximately two. Furthermore, the effect of the dissolved gases on density was not considered in the calculations. Based on the relationship between $F_{H,mix}$ and ΔT_{int} derived previously, the data of Newman would suggest a heat flux of 0.1 to 0.3 W m^{-2}. These heat fluxes correspond with the total heat fluxes that are required to explain the recent warming trend observed in the deep water. This comparison suggests that the deep-water warming could be explained by a limited heat transport via double-diffusive convection rather than by an increased heat input from external sources.

Effects of methane extraction on the double-diffusive structures The projected methane extraction plants are designed to withdraw water from depths between 300 and 400 m and to reinject the water after gas extraction at different depths. For the currently running pilot plant KP1, water is withdrawn from 320 m and reinjected at 90-m depth. The local monitoring team (T. Nzayisenga pers. comm.) observed that the water typically restratifies at around 100-m depth after dilution by ambient lake water. This leads to local positive peaks in temperature and CO_2 concentrations (indicated by negative peaks in pH), whereas the salinity of the diluted plume is similar to ambient concentrations at the restratification depth of ~100 m. The effects of this small-scale pilot plant on the double-diffusive staircases are negligible. The reinjected water restratifies above the double-diffusive staircases, and the withdrawal flow of 0.3 m^3 s^{-1} will not have a significant effect on the local stratification at 320-m depth. It would take almost 100 yr of continuous withdrawal at this rate to extract a 1-m-thick layer.

However, for the projected larger volume flows and deeper reinjection, significant effects can be expected. For example, at the withdrawal depth, the local gradients of temperature, dissolved substances, and density will be

enhanced. Consequently, this will increase the upward heat flux at this depth, which could lead to enhanced double-diffusive convection and the formation of a larger convectively mixed layer just above the extraction depth. At the restratification depth, the water in the reinjection plume will typically be warmer and contain more salts and CO_2 than the ambient water. As a consequence, an enhanced temperature gradient could support a strengthening of double-diffusive convection on the upper edge of the reinjection plume. Conversely, at the lower edge, salt fingers could appear.

Interaction between double diffusion and stratification In order to discuss the interaction between the double-diffusive convection and the large-scale stratification, we first summarize the vertical structure of the staircases using the data from the profile SE1. This profile contains 345 mixed layers within the depth range from 127.7 to 447.7 m, corresponding to an average layer density of 1.08 m ^{1}. Based on an average H_{mix} of 0.58 m, 200 m of the 320-m depth range (63%) consist of mixed layers. The 326 interfaces between consecutive mixed layers (average H_{int} of 0.167 m) contribute 54 m, or 17%. The other 20% (66 m) is either located in the main thermoclines or disturbed by inflows. The temperature difference over the whole depth range is 2.71 K. Of this, 1.53 K, or 56%, is covered by the temperature steps in the sharp interfaces, while the majority of the remaining temperature difference is included in the two gradient zones at 260- and 315-m depth.

The temperature gradient in the main thermocline between 255- and 262-m depth is $\sim$ 0.1 K m ^{1}, which is approximately three times the average temperature gradient in the interfaces (0.034 K m ^{1}) of the double-diffusive staircases. The molecular heat flux through the thermocline is therefore sufficient to remove the heat that is supplied by double-diffusive convection from below. Thus, the driving force forming the mixed layers is eliminated by the molecular heat flux, which explains the absence of staircases in the thermocline. Since H_{mix} decreases with increasing stability and the formation of mixed layers is suppressed by high temperature gradients, the average number of mixed layers per unit depth tends to be greatest in regions with an intermediate temperature gradient and N^2 of $\sim$ 10 ^{5} s ^{2} (Fig. 4).

In large sections of the water column, R_ρ is positively correlated with N^2 (Fig. 4). This indicates that heat is preferentially removed from regions with high density and temperature gradients. As a consequence, variations in the temperature gradient tend to be removed, which implies that the large-scale steplike structure of the temperature and density profiles (Fig. 2) is sustained by external forces.

In summary, our analysis reveals that the formation of the large-scale structure of the vertical profiles of temperature and dissolved substances is driven mainly by external sources. The discharge of these sources, which also drive the internal nutrient recycling, seems to have increased the recent past. Double-diffusive convection modifies the structure produced by the subaquatic sources. Generally, it levels out the steep gradients and removes heat from the deep water without removing a corresponding amount of dissolved salts and gases, thereby further stabilizing the stratification. In the long term, double-diffusion can be expected to remove any excess heat input into the deep water, increasing the energy required to destabilize the stratification and contributing to the safety of people living in the vicinity of the lake.

Acknowledgements

We thank the technicians M. Schurter and C. Dinkel as well as M. Halbwachs and B. Wehrli for their invaluable support during the preparation and the implementation of the measurements, B. Baluku and the captains and crew of the *Dakota* for their assistance during fieldwork, and L. C. Yee for data preparation. We also thank D. Kelley, N. Pasche, K. Ross, and an anonymous reviewer for their comments and suggestions for improving this manuscript. The fieldwork was supported by the United Nations Office for the Coordination of Humanitarian Affairs (OCHA) in order to evaluate the stability of the lake stratification in the aftermath of the Nyiragongo eruption in 2002 and by Eawag.

References

Chen, C. T., and F. J. Millero. 1986. Precise thermodynamic properties for natural waters covering only the limnological range. Limnol. Oceanogr. **31:** 657 662.

Degens, E. T., R. P. Von Herzen, H. K. Wong, W. G. Deuser, and H. W. Jannasch. 1973. Lake Kivu: Structure, chemistry and biology of an East African Rift Lake. Geol. Rundsch. **62:** 245 277.

Fedorov, K. N. 1988. Layer thicknesses and effective diffusivities in ''diffusive'' thermohaline convection in the ocean, p. 471 479. *In* J. C. J. Nihoul and B. M. Jamart [eds.], Small scale turbulence and mixing in the ocean. Elsevier.

Fernando, H. J. S. 1989. Oceanographic implications of laboratory experiments on diffusive interfaces. J. Phys. Oceanogr. **19:** 1707 1715, doi:10.1175/1520 0485(1989)019 <1707:OIOLEO>2.0.CO;2.

Gregg, M. C., and T. B. Meagher. 1980. The dynamic response of glass rod thermistors. J. Geophys. Res. **85:** 2779 2786.

Griffiths, R. W. 1979. The transport of multiple components through thermohaline diffusive interfaces. Deep Sea Res. **26:** 383 397.

Haberyan, K. A., and R. E. Hecky. 1987. The late pleistocene and holocene stratigraphy and paleolimnology of Lake Kivu and Tanganyika. Palaeogeogr. Palaeoclimatol. Palaeoecol. **61:** 169 197, doi:10.1016/0031 0182(87)90048 4.

Hoare, R. A. 1966. Problems of heat transfer in Lake Vanda, a density stratified arctic lake. Nature **210:** 787 789, doi:10.1038/ 210787a0.

Kelley, D. E. 1990. Fluxes through diffusive staircases: A new formulation. J. Geophys. Res. **95:** 3365 3371.

, H. J. S. Fernando, A. E. Gargett, J. Tanny, and E. Oezsoy. 2003. The diffusive regime of double diffusive convection. Prog. Oceanogr. **56:** 461 481, doi:10.1016/ S0079 6611(03)00026 0.

Kocsis, O., H. Prandke, A. Stips, A. Simon, and A. Wuest. 1999. Comparison of dissipation of turbulent kinetic energy determined from shear and temperature microstructure. J. Mar. Syst. **21:** 67 84, doi:10.1016/S0924 7963(99)00006 8.

Kunze, E. 2003. A review of oceanic salt fingering theory. Prog. Oceanogr. **56:** 399 417, doi:10.1016/S0079 6611(03)00027 2.

Lide, D. R. [ed.]. 2009. CRC handbook of chemistry and physics, Internet version (89th ed.). Taylor and Francis. Available from http://www.hbcpnetbase.com

Lorke, A., K. Tietze, M. Halbwachs, and A. Wuest. 2004. Response of Lake Kivu stratification to lava inflow and climate warming. Limnol. Oceanogr. **49:** 778 783.

Matzner, R. A. 2001. Dictionary of geophysics, astrophysics and astronomy. CRC Press.

Mudge, T. D., and R. G. Lueck. 1994. Digital signal processing to enhance oceanographic observations. J. Atmos. Oceanic Technol. **11:** 825 836, doi:10.1175/1520 0426(1994)011 <0825:DSPTEO>2.0.CO;2

Muvundja, F. A., and others. 2009. Balancing nutrient inputs to Lake Kivu. J. Gt. Lakes Res. **35:** 406 418, doi:10.1016/ j.jglr.2009.06.002.

Newman, F. C. 1976. Temperature steps in Lake Kivu: A bottom heated saline lake. J. Phys. Oceanogr. **6:** 157 163.

Onken, R., and E. Brambilla. 2003. Double diffusion in the Mediterranean Sea: Observation and parameterization of salt finger convection. J. Geophys. Res. **108:** 8124, doi:10.1029/ 2002JC001349.

Padman, L., and T. M. Dillon. 1987. Vertical heat fluxes through the Beaufort Sea thermohaline staircase. J. Geophys. Res. **92:** 10799 10806, doi:10.1029/JC092iC10p10799.

Pasche, N., C. Dinkel, B. Muller, M. Schmid, A. Wuest, and B. Wehrli. 2009. Physical and biogeochemical limits to internal nutrient loading of meromictic Lake Kivu. Limnol. Oceanogr. **54:** 1863 1873.

Powell, T., and A. Jassby. 1974. The estimation of vertical eddy diffusivities below the thermocline in lakes. Water Resour. Res. **10:** 191 198.

Sánchez, X., and E. Roget. 2007. Microstructure measurements and heat flux calculations of a triple diffusive process in a lake within the diffusive layer convection regime. J. Geophys. Res. **112:** C02012, doi:10.1029/2006JC003750.

Schmid, M., M. Halbwachs, B. Wehrli, and A. Wuest. 2005. Weak mixing in Lake Kivu: new insights indicate increas ing risk of uncontrolled gas eruption. Geochem. Geophys. Geosyst. **6:** Q07009, doi:10.1029/2004GC000892.

, A. Lorke, C. Dinkel, G. Tanyileke, and A. Wuest. 2004a. Double diffusive convection in Lake Nyos, Cameroon. Deep Sea Res. I **51:** 1097 1111, doi:10.1016/j.dsr.2004.02. 010.

, K. Tietze, M. Halbwachs, A. Lorke, D. McGinnis, and A. Wuest. 2004b. How hazardous is the gas accumulation in Lake Kivu? Arguments for a risk assessment in light of the Nyiragongo Volcano eruption of 2002. Acta Vulcanol. **14/15:** 115 121.

Schmitt, R. W., J. R. Ledwell, E. T. Montgomery, K. L. Polzin, and J. M. Toole. 2005. Enhanced diapycnal mixing by salt fingers in the thermocline of the tropical Atlantic. Science **308:** 685 688, doi:10.1126/science.1108678.

Sigurdsson, H., J. D. Devine, F. M. Tchoua, T. S. Presser, M. K. W. Pringle, and W. C. Evans. 1987. Origin of the lethal gas burst from Lake Monoun, Cameroun. J. Volcanol. Geotherm. Res. **31:** 1 16, doi: 10.1016/0377 0273(87)90002 3.

Sigvaldason, G. E. 1989. International Conference on Lake Nyos Disaster, Yaounde, Cameroon 16 20 March, 1987 conclu sions and recommendations. J. Volcanol. Geotherm. Res. **39:** 97 107, doi:10.1016/0377 0273(89)90050 4.

Tassi, F., and others. 2009. Water and gas chemistry at Lake Kivu (DRC): Geochemical evidence of vertical and horizontal heterogeneities in a multibasin structure. Geochem. Geophys. Geosyst. **10:** Q02005, doi:10.1029/2008GC002191.

Tietze, K. 1978. Geophysical examination of Lake Kivu and its unusual methane deposit: Stratification, dynamics and gas content of the lake water. Ph.D. thesis. Christian Albrechts Universität Kiel (written in German).

Timmermans, M. L., J. Toole, R. Krishfield, and P. Winsor. 2008. Ice tethered profiler observations of the double diffusive staircase in the Canada Basin thermocline. J. Geophys. Res. **113:** C00A02, doi:10.1029/2008JC004829.

Turner, J. S. 1965. The coupled turbulent transports of salt and heat across a sharp density interface. Int. J. Heat Mass Transfer **8:** 759 767.

. 1973. Buoyancy effects in fluids. Cambridge University Press.

Associate editor: Robert E. Hecky

Received: 08 April 2009
Accepted: 09 August 2009
Amended: 28 August 2009